IMU-based Monitoring of Buoy-Ballast System through Cable Dynamics Simulation

Charly Peraud, Martin Filliung, Cédric Anthierens, Claire Dune, Nicolas Boizot, Vincent Hugel

IMU-based Monitoring of Buoy-Ballast System through Cable Dynamics Simulation

Charly Peraud[1], Martin Filliung[1,2], Cédric Anthierens[1], Claire Dune[1], Nicolas Boizot[2], Vincent Hugel[1]

***Abstract*— This study is twofold. First, a comprehensive simulation framework of cable dynamics is introduced. This framework considers variable length cables and allows to incorporate elements such as buoys, ballast or Inertial Measurement Unit (IMU) sensors. The accuracy of this framework is assessed through experimental data. Second, a novel and improved solution for the instrumentation of a V-shaped buoy-ballast system using IMU sensors is investigated. This latter, designed for a neutrally buoyant tether between a Remotely Operated Vehicle (ROV) and an Unmanned Surface Vehicle (USV), is meant to improve operation safety. The discussed IMU-based solution provides wider information on the interaction between the ROV and the cable, including its 3D orientation and curvature amplitude, which could be used for both the control of the USV trajectory and its onboard winch.**

I. Introduction

To ensure the safe operation of underwater vehicles tethered to a follower USV, the umbilical must be carefully managed. Indeed, it needs to be appropriately released by means of a winch, without excessive tensions or letting the cable go slack.

In response to these challenges, prior studies [1], [2] introduced a compliant buoy-ballast system integrated on a neutrally buoyant tether, illustrated in Fig. 1. This innovative system consists of two buoys spaced 120 cm apart, with a ballast positioned precisely between them, forming a balanced "V-shape" at rest, creating compliance in the system. Incorporating a flex sensor at the ballast enabled the V-shaped system to measure local curvature, which was used to estimate the distance between buoys through interpolated data tables. This sensor signal fed the winch controller to release cable length on demand. Both buoys and the ballast were engineered to achieve overall neutral buoyancy in water, thereby functioning as a damping mechanism to counteract external perturbations induced by the cable on the ROV.

This study extends the analysis of the buoy-ballast system described above by enhancing its sensing capacities, with the aim of obtaining additional information about the cable behavior near the ROV. In addition to the inter-buoy distance, the replacement of the flex sensor with IMU sensors attached to this system can provide measurements of 3D orientation and amplitude of curvature, and help to determine the direction of tension, which can be caused by ROV movements, winch action or cable drift. The knowledge of the cable configuration will be useful to control the trajectory of a follower USV and its onboard winch for automatically managing the umbilical throughout ROV exploration missions.

[1]COSMER Laboratory, Univ. de Toulon, France
[2]Univ. de Toulon, Aix Marseille Univ, CNRS LIS, Marseille, France

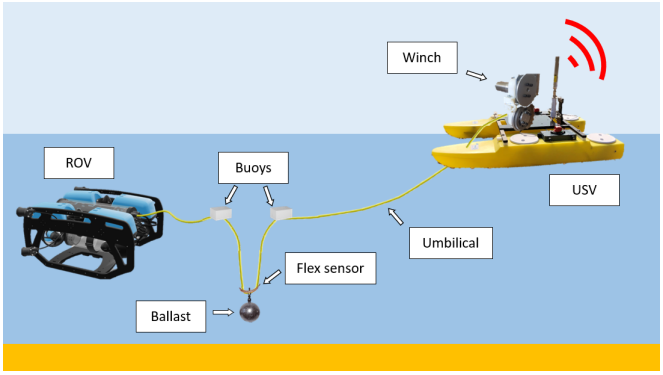

Fig. 1. Compliant buoy-ballast system integrated on the umbilical of a ROV/USV system.

In order to conduct such a study in simulation, the specifications that the simulator must meet are listed below.

- the cable must be modeled with its own mechanical characteristics (stiffness, diameter, mass, volume).
- it must be possible to add buoys, ballasts or virtual sensors such as IMUs at any position on the cable,
- cable length must be controlled by the simulation of the winding function of a virtual winch,
- the simulator must be executable as an internal model to improve future on-line control of the USV trajectory. Therefore internal computation data must be available to any external control algorithm,
- it must be possible to start simulations from a given physically admissible configuration of the whole system including the USV, ROV and umbilical.

The use of this simulator helps to determine the number of IMU sensors and their most relevant position on the cable. Simulator solutions exist, such as Matlab/Simulink, Vortex [1], UUV Simulator [3], SOFA [4] but none of them meet all these requirements. Therefore, a novel comprehensive simulation framework is introduced as a solution to conduct an in-depth analysis of the V-shaped system.

This paper is organized as follows. Section II provides a review of related works in the field. Section III presents the modeling approach and details the simulation framework. Section IV outlines the validation procedures to check the accuracy and reliability of the simulator. Section V will discuss the benefits of employing a novel IMU-based solution for the V-shaped system, looking at the results of round trip, turn and dive simulations. Finally, Section VI concludes the study and presents future research prospects.

II. Related work

Various models are commonly employed to approximate the shape of a weighty cable, including the catenary [5] or the parabolic [6] shape, particularly useful for localization applications in both air [7] and water [8]. However, they reach their limitations when cable motion is dynamic [9] and are only consistent with cables subject to significant hydrostatic forces, either heavy or buoyant. In other cases, the use of a more comprehensive model becomes necessary.

Several methods exist for modeling cable dynamics [10]. The Finite Element Method (FEM) offers increased precision and can handle complex geometries, although it suffers from computational complexity [11], [12]. The Finite Difference Method (FDM), which approximates governing equations of a cable, is better suited for simpler shapes, although its overall accuracy is lower than FEM [13], [14]. The Kane's method provides a simplified approach, treating cables as one-dimensional elements with negligible bending stiffness, suitable for scenarios where flexibility is less critical [15], [16]. Conversely, the Cosserat method accounts for intrinsic flexibility and torsion, making it suitable for scenarios where these effects are significant, such as modeling flexible systems or systems under complex constraints [17].

Few works explore buoy-ballast immersed systems. Solutions based on sliding elements of positive and negative buoyancy along the cable are investigated to maintain linear shapes, though at the expense of the forces exerted on the ROV [18]. Marine Submersible Buoys solutions are widely used for various purposes in marine environments, where they can act as mooring systems, oceanographic instruments, or communication stations [19], [20].

The simulation framework developed in this work model cable dynamics using the FDM, which offer a balance between computational simplicity and acceptable accuracy.

III. Modeling

Let us consider a variable-length cable that has one extremity connected to the onboard winch of an USV and the other extremity to a ROV through a virtual ball joint.

A. Underwater Cable Model

The cable is assumed to be homogeneous and isotropic, implying consistent mechanical properties across all directions and points. A linear elasticity model, based on Hooke's law, is adopted, assuming tensions to remain within the cable's elastic domain limit. In addition, torsion effects are not taken into account.

Let us define $B_w = (\boldsymbol{x}, \boldsymbol{y}, \boldsymbol{z})$ as an orthonormal vector basis with the vertical $\boldsymbol{z}$-axis oriented upwards, and $R_w = (O_w, B_w)$ as a fixed reference frame with origin O_w. Following [13], t is the time variable, s and S denote the cable's unstretched and stretched curvilinear abscissa respectively. Each point P_s is associated with an orthonormal vector local basis $B^{t,s} = (\boldsymbol{t}^{t,s}, \boldsymbol{n}^{t,s}, \boldsymbol{b}^{t,s})$ and a local frame $R^{t,s} = (P_s, B^{t,s})$, where $\boldsymbol{t}^{t,s}$ represents the unit tangent vector to the cable at P_s, $\boldsymbol{n}^{t,s}$ is orthogonal to $\boldsymbol{t}^{t,s}$, and $\boldsymbol{b}^{t,s} = \boldsymbol{t}^{t,s} \times \boldsymbol{n}^{t,s}$. This local frame is oriented by two angles $\theta^{t,s}$, $\phi^{t,s}$, as illustrated in Fig 2, considering $\psi = -\frac{\pi}{2}$, to place $\boldsymbol{n}^{t,s}$ in the direction of $-\boldsymbol{z}$ if $\theta^{t,s} = \phi^{t,s} = 0$.

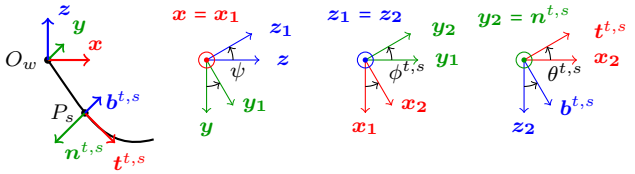

Fig. 2. Definition of $R^{t,s}$ with respect to R_w

According to [13], the cable's dynamic state at P_s can be expressed with one internal tangential force variable $T_t^{t,s}$, three velocity variables $V_t^{t,s}$, $V_n^{t,s}$, $V_b^{t,s}$ and two orientation variables $\theta^{t,s}$, $\phi^{t,s}$. To account for bending stiffness, two internal normal force variables $T_n^{t,s}$, $T_b^{t,s}$ are introduced. The resulting dynamic state vector $\boldsymbol{Y^{t,s}}$ is defined as follows

$$\boldsymbol{Y^{t,s}} = \left[T_t^{t,s}, T_n^{t,s}, T_b^{t,s}, V_t^{t,s}, V_n^{t,s}, V_b^{t,s}, \theta^{t,s}, \phi^{t,s}\right]^T \quad (1)$$

An equal number of independent equations is required to solve the cable's dynamic behavior, leading to the formulation of three types of equations,

- relative to the linear balance of forces,

$$\frac{\partial}{\partial S}\boldsymbol{T}^{t,s} + \boldsymbol{W}^{t,s} + \boldsymbol{F}^{t,s} + \boldsymbol{B_A}^{t,s} = \boldsymbol{0} \quad (2)$$

  $\boldsymbol{T}^{t,s}$ is the cable's internal forces vector at P_s, $\boldsymbol{W}^{t,s}$ is the linear hydrostatic forces vector, $\boldsymbol{F}^{t,s}$ is the linear cable drag forces vector, accounting marine currents' influence, and $\boldsymbol{B_A}^{t,s}$ is the linear d'Alembert forces vector governing cable motion, which considers the effects of acceleration quantity and added mass.
- relative to the compatibility relationship, to ensure the continuous dependency of the position vector $\boldsymbol{P_s}$ on both t and s :

$$\frac{\partial}{\partial s}\frac{\partial}{\partial t}\boldsymbol{P_s} = \frac{\partial}{\partial t}\frac{\partial}{\partial s}\boldsymbol{P_s} \quad (3)$$

- relative to the angular momentum theorem, to incorporate bending stiffness, using a first-order approximation,

$$\boldsymbol{t}^{t,s} \times \boldsymbol{T}^{t,s} + \frac{\partial}{\partial S}\boldsymbol{M_f}^{t,s} = \boldsymbol{0} \quad (4)$$

  This involves applying the flexion moment relation :

$$\boldsymbol{M_f}^{t,s} = EI\boldsymbol{t}^{t,s} \times \frac{\partial \boldsymbol{t}^{t,s}}{\partial S} \quad (5)$$

  Here, E represents the Young modulus, and I is the moment of inertia of the cable section.

In addition, boundary conditions are introduced to deal with the cable's attachment to robots at both ends. The robots' control directly enforces velocities $V_t^{t,0}$, $V_n^{t,0}$, $V_b^{t,0}$, $V_t^{t,L}$, $V_n^{t,L}$, $V_b^{t,L}$ $\forall t$, with L representing the currently deployed length. Additionally, the ROV connection is left free of bending, enforcing values for $T_n^{t,0}$, $T_b^{t,0}$, using a virtual link aligned with the previous one. The desired orientation of the cable on the USV side, denoted as $\theta^{t,L}$ and $\phi^{t,L}$, is set to match the output of the winch cable.

TABLE I

DYNAMIC DISCRETE EQUATIONS BASED ON N POINTS

Type of equation	Number of discrete equations
Balance of Forces (BoF)	$3(N-1)$
Compatibility Relationship (CR)	$3(N-1)$
Angular Momentum Theorem (AMT)	$2(N-2)$
Velocity boundary conditions	6
Rigid start point boundary conditions	4

B. Numerical Methods and Resolution

The cable is discretized into N points, so that all points are spaced d_{s_0} apart, excepted the distance $d_{P_{N-2}P_{N-1}}$ which is constrained within $[d_{s_{min}}, d_{s_{max}}]$, offering flexibility in cable length. The full dynamic state vector $\boldsymbol{Y^t}$ is a $8N$ vector :

$$\boldsymbol{Y^t} = \left[\boldsymbol{Y^{t,0}}^T, \boldsymbol{Y^{t,1}}^T, \dots, \boldsymbol{Y^{t,N-1}}^T\right]^T \tag{6}$$

To numerically solve cable dynamics, $8N$ independent equations are necessary, involving partial derivatives with respect to time and space. A Finite Difference approximation Method is employed for this purpose, which necessitates $i+1$ points to approximate the i^{th} partial derivative. Therefore, based on N points, the balance of forces and the compatibility relationship each yields $3(N-1)$ equations. The angular momentum theorem, relying on second-order space partial derivatives, yields $2(N-2)$ equations. Boundary conditions contribute an additional 10 equations, totaling $8N$ equations as summarized in Table I.

A Newton-Raphson iteration algorithm is used for solving, starting from a compatible initial configuration, with a time step dt. The initial configuration can be defined in different ways, using a taut shape or a catenary cable shape, or by adopting a pre-simulated dynamic state, assuming that the desired initial shape and motion are specified, which includes velocities, accelerations, and orientations at each point. The $3N$ internal forces are determined by assuming negligible variation of internal forces over a short time period dt and using a least-squares method on the resulting $5N-7$ equations derived from BoF and AMT equations (Table I).

To address length variations induced by the winch during the cable management, the methodology proposed in [21] is adopted. This involves considering that P_0 is attached to the ROV, and P_{N-1} is attached to the winch. During reel-in and pay-out operations, a tangential speed is added to the $V_t^{t,N-1}$ boundary condition based on the winch speed when solving the system. For the final point to be aligned with the winch's real position, it is required to recalculate its s-value and interpolate the state vector of P_{N-1} using the previous resolved values at the updated s-value. If $d_{P_{N-2}P_{N-1}}$ falls outside the prescripted distance range constraint, adjustments are necessary. If $d_{P_{N-2}P_{N-1}} > d_{s_{max}}$, a new point P_s is added d_{s_0} away from P_{N-2}, making P_N the starting point of the winch and setting $P_{N-1} = P_s$. Conversely, if $d_{P_{N-2}P_{N-1}} < d_{s_{min}}$, P_{N-2} is removed to avoid compression, and P_{N-1} becomes P_{N-2}.

TABLE II

TRAJECTORIES' DESCRIPTION

Trajectory	1	2	3	4	5	6
Distance [m]	2	2	1.5	2	1.5	2
Motion	surge	surge	sway	sway	sway	sway
Speed [m/s]	0.25	0.5	0.25	0.25	0.5	0.5

The model incorporates the discrete addition of elements, such as buoys or ballasts, at specific points. Consequently, when an element is added to point P_s, additional terms reflecting the impact of this element are included to augment the values of $\boldsymbol{W}^{t,s}$, $\boldsymbol{F}^{t,s}$, and $\boldsymbol{B}^{t,s}$.

IV. VALIDATION

A. Comparison with Experimental Data

Experiments described and illustrated in a previous work [9] were conducted to track the positions of multiple weighty cables over time during robot motion using an underwater motion tracking system as ground truth. Optical markers were attached to both the robot and each cable, evenly spaced out by 20 cm (16 markers for a 3-meter-long cable). The recorded datasets were utilized to assess the motion accuracy of the model.

Simulations are carried out (see an example at https://youtu.be/jEm2rzcwzj0) using a spatial step size of 5 cm and incorporating the cable's physical and mechanical attributes, such as density and diameter. A 3-meter-long leaded seamstress rope, referred to as cable 6 in [9], is subject to six distinct ROV movements, as detailed in Table II. The initial shape of the simulated cable is interpolated from the initial positions of all points tracked by the motion capture system, while the velocity boundary conditions at the cable's ends are updated based on the discrete derivative of their time-varying positions.

The difference between the ground truth data and the simulated data leads a residual named $\varepsilon^{t,s}$. Statistical analyses are conducted for each trajectory, considering all residual values across both time and space dimensions denoted as $\mathbb{T}$ and $\mathbb{S}$, respectively, with each trajectory performed three times. For an experiment indexed by k, the residual vector $\boldsymbol{\varepsilon_k}$ is defined as

$$\boldsymbol{\varepsilon_k} = \left[\varepsilon^{t,s} \mid t \in \mathbb{T}, s \in \mathbb{S}\right] \tag{7}$$

Percentile values provide a more accurate representation of a data distribution that deviates from a Gaussian distribution. The i^{th} percentile value, namely $P_{i^{th}}$, is the value below which $i\%$ of the data points lie. Common percentiles include the median $P_{50^{th}}$, the first quartile $P_{25^{th}}$, and the third quartile $P_{75^{th}}$. The $P_{1^{th}}$ and $P_{99^{th}}$ percentiles are used instead of the minimum and maximum values to mitigate the impact of outliers in the analysis. The percentiles obtained are presented in Table III. As a result, over 99% of residuals, encompassing dynamic stages, are below 25 mm, which is an acceptable level of precision for a 3-meter-long cable.

TABLE III

PERCENTILES OF TRAJECTORIES' RESIDUALS [MM]

Trajectory	1	2	3	4	5	6
$P_{1^{th}}$	0.08	0.01	0.09	0.08	0.47	0.13
$P_{25^{th}}$	3.96	8.16	3.86	3.78	5.85	6.95
$P_{50^{th}}$	9.32	12.91	10.62	12.24	12.38	12.02
$P_{75^{th}}$	13.31	16.50	15.40	15.63	15.80	14.94
$P_{99^{th}}$	18.98	24.26	21.85	22.10	22.59	21.34

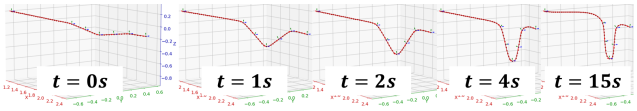

Fig. 3. Buoy-ballast system stabilizing around resting position

B. Compliant Buoy-Ballast System on Simulation

The V-shaped system was replicated in the simulator. A preliminary simulation (https://youtu.be/1dYweIBYVUg) was conducted to converge to the resting configuration, to check its similarity to the real system. The resting configuration setup will serve as the initial condition for subsequent simulations, allowing the observation of the response of the V-shaped system to different scenarios, including the ROV moving away, the winch reeling in, or both actions. At the beginning of this simulation, the cable is pre-tensioned, with a fixed length while the ROV moves backward. The neutral cable used (Fathom Slim tether from BlueRobotics™) has a 4 mm diameter and its stiffness was determined in [1]. As the simulation progresses, using the same step size as in Section IV-A, the system gradually takes on its characteristic V shape, eventually stabilizing around a static equilibrium position (Fig. 3). Considering the mechanical properties of the buoys and ballast, the theoretical distance between the buoys in the resting configuration of the V-shaped system is approximately 22 cm [2]. At the end of the simulation, the cable remains slightly taut, with an inter-buoy distance of about 22 cm. Given the cable's neutral buoyancy, it naturally tends to minimize the bending energy towards a shape that smooths the curvature outside the V-shaped system.

V. IMU-BASED MONITORING

A. Simulation Setup

Several simulations were conducted in our simulation framework incorporating the buoy-ballast system previously modeled, with one end of the cable tethered to a ROV and the other end fixed to a controlled winch (Fig. 4). The ROV is modeled with three trapezoidal velocity profiles for its degrees of freedom (surge, yaw and heave), parameterized by waypoints. The winch is actuated according to the buoy-gap control mode described in [1], employing a proportional-derivative controller. As the natural inter-buoy distance of the V-shaped system is related to the buoys' speed [2], updates to the desired inter-buoy distance are made during winch control. The simulations start at equilibrium (Fig. 3), and three distinct trajectories were tested for the ROV :

- Round Trip : forward and backward surge motion.

TABLE IV

ROV WAYPOINTS [TIME, SURGE, HEAVE OR YAW]

UNITS: TIME $[s]$; SURGE,HEAVE $[m/s]$; YAW $[rad/s]$

Trajectory	Round Trip	Turn	Dive
Waypoint	[t, s]	[t, s, y]	[t, s, h]
0	[0, 0]	[0, 0, 0]	[0, 0, 0]
1	[2, 0.2]	[1, 0.2, 0]	[2, 0.2, 0]
2	[4, 0.2]	[2, 0.2, 0]	[4, 0.2, 0]
3	[6, 0]	[3, 0.2, −0.4]	[6, 0.2, −0.2]
4	[12, 0]	[6, 0.2, −0.4]	[8, 0.2, −0.2]
5	[14, −0.2]	[7, 0.2, 0]	[10, 0, 0]
6	[16, −0.2]	[8, 0.2, 0]	[15, 0, 0]
7	[18, 0]	[10, 0, 0]	-
8	[24, 0]	[15, 0, 0]	-

- Turn : combined forward surge and yaw motion.
- Dive : combined forward surge and heave motion.

These trajectories allow seeing the V-shaped system's behavior in either basic or more realistic movements, and their ROV waypoints are described in Table IV.

Additionally, in order to check the advantages of a novel instrumentation, five IMUs were placed along the cable, one on the ballast, one on each buoy, and the remaining two between each buoy and ballast (Fig 4). The IMUs, modeling I2C BMX160 9-axis IMUs from DFRobot[1], are designed with an axis that is collinear with the normal vector to the cable's section, which will be referred to as its tangential axis. The IMU data were reconstructed by using the resolved values of velocities and orientations obtained during the simulation, augmented by the gravitational acceleration. It is assumed that the orientations provided by the IMUs are not affected by gyro drifts ($\approx 0.01°/s$), as this drift appears to be negligible during the few-second dynamic phase of the V-shape system.

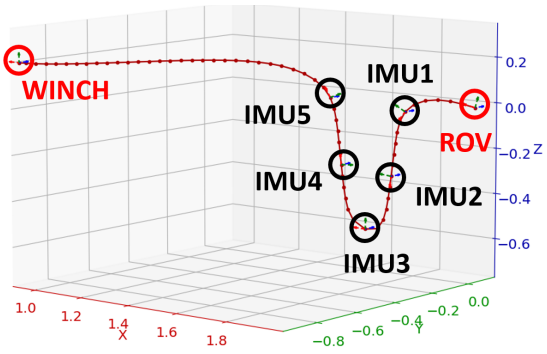

Fig. 4. IMUs placement on the V-shaped system (simulator view)

B. Reconstructed data

In order to observe the V-shaped system's configuration, several relevant signals are estimated using IMUs data, and compared with simulated data.

- *Inter-buoy distance :* The orientation of the i^{th} IMU is used to get the coordinates of its tangent vector.

$$\boldsymbol{t_i} = \left[\cos\boldsymbol{\phi_i}\cos\boldsymbol{\theta_i}, -\sin\boldsymbol{\theta_i}, -\sin\boldsymbol{\phi_i}\cos\boldsymbol{\theta_i}\right]^T_{R_w} \quad (8)$$

[1]https://wiki.dfrobot.com/BMX160_9_Axis_Sensor_Module_SKU_SEN0373

Assuming that the cable remains straight between each buoy and the ballast with a fixed distance d_{BB_A} of 0.6 m, an estimation of the distance between the buoys $\boldsymbol{d_{BB}}$ is obtained, using $\boldsymbol{t_2}$ and $\boldsymbol{t_4}$:

$$\boldsymbol{d_{BB}} = ||d_{BB_A}.\boldsymbol{t_2} + d_{BB_A}.\boldsymbol{t_4}|| \tag{9}$$

- *Curvature :* The analytic curvature vector $\boldsymbol{\gamma_i}$ is obtained by deriving $\boldsymbol{t_i}$ with respect to s :

$$\boldsymbol{\gamma_i} = \left[0, \frac{\partial \boldsymbol{\phi_i}}{\partial s} \cos \boldsymbol{\theta_i}, -\frac{\partial \boldsymbol{\theta_i}}{\partial s}\right]^T_{R_i} \tag{10}$$

As it depends on derivative variables, its discrete value $\boldsymbol{\gamma_{ij}} = (0, \boldsymbol{\gamma^n_{ij}}, \boldsymbol{\gamma^b_{ij}})$ is expressed at the central point between two consecutive IMUs $(i < j)$:

$$\boldsymbol{\gamma_{ij}} = \left[0, \frac{\boldsymbol{\phi_j} - \boldsymbol{\phi_i}}{s_j - s_i} \cos \frac{\boldsymbol{\theta_i} + \boldsymbol{\theta_j}}{2}, -\frac{\boldsymbol{\theta_j} - \boldsymbol{\theta_i}}{s_j - s_i}\right]^T_{R_{\frac{i+j}{2}}} \tag{11}$$

- *Turning angle :* The scalar product of the horizontal projections of vectors $\boldsymbol{t_i}$ and $\boldsymbol{t_{ROV}}$ gives angles, named $\boldsymbol{\alpha_i}$, which are useful to track the cable horizontal turning angle with respect to the ROV.

C. Results

Figures 5, 6, and 7 display IMU-based estimated distance and simulated distance, simulated cable tension at buoys, estimated curvature and simulated curvature on the right-hand side of the lest (between IMU 2 and IMU 3), for the Round Trip, Turn and Dive simulations. Horizontal angles are also displayed for the Turn simulation.

In all three simulations, the IMU-based estimated inter-buoy distance and the simulated one show similar variations, although a deviation is observable. This comes from the approximation of the cable part between the buoy and the ballast as a rigid segment, which becomes more precise as the cable gets straighter, as highlighted in Fig. 7.

The tangential cable tension difference, namely ΔTt_{15}, between the buoys appears to be rather in phase with the inter-buoy distance. However, they are linked by a nonlinear relationship that includes the 1st and 2nd order derivatives

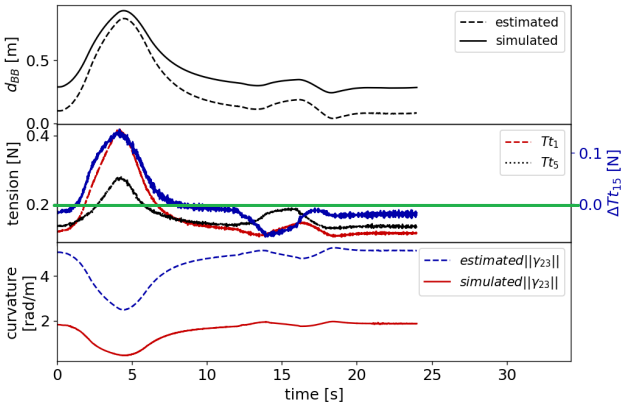

Fig. 5. Inter-buoy distance (IMU-based and simulated), tension at buoys (simulated), curvature (IMU-based and simulated) signals during round trip simulation, published online in March 2024, https://youtu.be/0JbwC3mf4dc

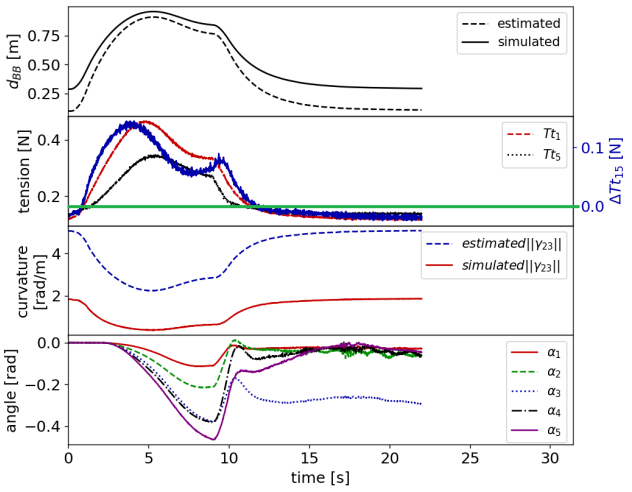

Fig. 6. Inter-buoy distance (IMU-based and simulated), tension at buoys (simulated), curvature (IMU-based and simulated), horizontal angle (simuated) signals during turn simulation, published online in March 2024, https://youtu.be/xx91qPXUkgw

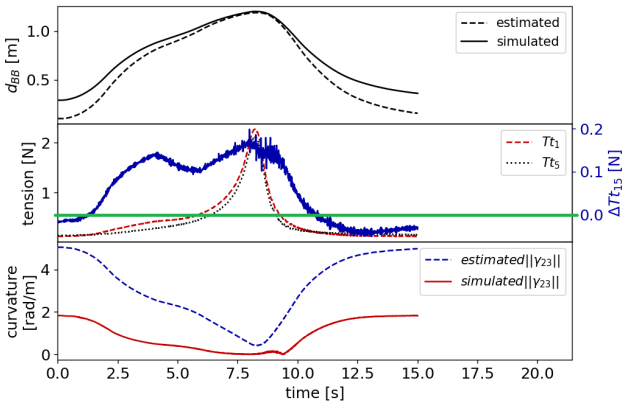

Fig. 7. Inter-buoy distance (IMU-based and simulated), tension at buoys (simulated), curvature (IMU-based and simulated) signals during dive simulation, published online in March 2024, https://youtu.be/XwsexYf5loo

of the distance, which are responsible for the local variation differences between both quantities. It is possible to estimate the tension difference more accurately from the dynamic equations of the buoys, the ballast, and the buoy-ballast cable portions modeled as rigid segments. The sign of the estimated tension difference allows determining the pulling direction of the cable, i.e. whether the ROV or the USV winch is responsible for the pulling action.

The IMU-based curvature near the ballast is computed through the previous curvature formula, using IMU2, IMU3 and IMU4 (Fig. 4). The curvature magnitude reflects the available compliance capacity of the V-shaped system. The tauter the cable, the less curvature is to be detected. As the curvature is similar at both side of the ballast, only $||\gamma_{23}||$ is represented. The variations of the simulated signal are less pronounced than the variations of the IMU-based estimated signal, which becomes a coarser approximation as the V-system tightens up.

The IMU-based turning angle relative to the ROV direction is relevant in the turn simulation, which indicates that the V-

shape does not remain in the same vertical plane. To take into account such a curved trajectory, the winch speed will have to be reduced. Moreover, after the ROV has stopped, the V-shape tends to fit back again into a vertical plane that does not include the rest of the cable, as highlighted during the turn simulation. This can be explained by the fact that the bending moments at the buoys are counteracting each other, which prevent the V system from realigning with the overall cable. When the umbilical becomes too slack, the V-shape may turn around the vertical axis, increasing the inter-buoy distance, and consecutively commanding the winch to release even more cable length. Thus, the detection of out-of-plane configurations of the V-shaped system will contribute to improve the cable management.

VI. Conclusion

This study focuses on the analysis of a novel instrumentation based on IMU sensors to equip a compliant buoy-ballast system on a neutrally buoyant underwater cable. The accuracy of this simulation framework has been assessed by comparing simulated data with real data recorded using the Qualisys motion tracking system during experiments conducted in a water tank.

Forward/backward, turn and dive simulations of the ROV were carried out, while the winch was controlled based on the distance between the buoys. The simulated system appears to behave similarly to the experimental videos documented in [2]. The IMU-sensor envelope allows estimating the inter-buoy distance (already provided by the flex sensor), the curvature near the ballast, and potentially the cable tension difference at the buoys, which can be useful to set up a more efficient cable length control for the USV winch. Moreover, it facilitates the identification of possible out-of-plane configurations of the V-shaped system through the estimation of the turning angle, enabling adjustments to the control of both a follower USV and its winch as necessary.

Future work will focus on designing and implementing this novel instrumentation to improve the control of the overall system during ROV missions, in order to gain maneuverability. To achieve this, the simulation framework will be enhanced by incorporating hydrodynamic models of robots. External disturbances will also be introduced, such as marine current maps, to simulate real-world operating conditions.

References

[1] Ornella Tortorici, Cédric Anthierens, and Vincent Hugel. A New Flex-Sensor-Based Umbilical-Length Management System for Underwater Robots. In *2023 European Conference on Mobile Robots (ECMR)*, pages 1–6, Coimbra, Portugal, September 2023. IEEE.

[2] Ornella Tortorici, Charly Péraud, Cédric Anthierens, and Vincent Hugel. Automated Deployment of an Underwater Tether Equipped with a Compliant Buoy–Ballast System for Remotely Operated Vehicle Intervention. *Journal of Marine Science and Engineering*, 12(2):279, February 2024.

[3] Musa Morena Marcusso Manhães, Sebastian A. Scherer, Martin Voss, Luiz Ricardo Douat, and Thomas Rauschenbach. UUV simulator: A gazebo-based package for underwater intervention and multi-robot simulation. In *OCEANS 2016 MTS/IEEE Monterey*. IEEE, sep 2016.

[4] F. Faure, C. Duriez, H. Delingette, J. Allard, B. Gilles, S. Marchesseau, H. Talbot, H. Courtecuisse, G. Bousquet, I. Peterlik, and S. Cotin. SOFA: A Multi-Model Framework for Interactive Physical Simulation. In Yohan Payan, editor, *Soft Tissue Biomechanical Modeling for Computer Assisted Surgery*, volume 11 of *Studies in Mechanobiology, Tissue Engineering and Biomaterials*, pages 283–321. Springer, June 2012.

[5] Juliette Drupt, Claire Dune, Andrew I. Comport, and Vincent Hugel. Validity of the catenary model for moving submarine cables with negative buoyancy. In *3rd workshop on RObotic MAnipulation of Deformable Objects: challenges in perception, planning and control for Soft Interaction (ROMADO-SI),*, Kyoto, Japan, October 2022.

[6] Lev Smolentsev, Alexandre Krupa, and François Chaumette. Shape visual servoing of a tether cable from parabolic features. In *2023 IEEE International Conference on Robotics and Automation (ICRA)*, pages 734–740, London, United Kingdom, May 2023. IEEE.

[7] A. Borgese, D. C. Guastella, G. Sutera, and G. Muscato. Tether-Based Localization for Cooperative Ground and Aerial Vehicles. *IEEE Robotics and Automation Letters*, 7(3):8162–8169, July 2022. Conference Name: IEEE Robotics and Automation Letters.

[8] J. Drupt, C. Dune, A. I. Comport, S. Sellier, and V. Hugel. Inertial-Measurement-Based Catenary Shape Estimation of Underwater Cables for Tethered Robots. In *2022 IEEE/RSJ International Conference on Intelligent Robots and Systems (IROS)*, October 2022.

[9] M. Filliung, J. Drupt, C. Peraud, C. Dune, N. Boizot, A. Comport, C. Anthierens, and V. Hugel. An Augmented Catenary Model for Underwater Tethered Robots. In *IEEE Int. Conf. on Robotics and Automation (ICRA 2024)*, Yokohama, Japan, May 2024.

[10] Z. H. Zhu. Dynamic modeling of cable system using a new nodal position finite element method. *International Journal for Numerical Methods in Biomedical Engineering*, 26(6):692–704, 2010.

[11] Ole Alexander Nørve Eidsvik and Ingrid Schjølberg. Finite element cable-model for Remotely Operated Vehicles (ROVs) by application of beam theory. *Ocean Engineering*, 163:322–336, September 2018.

[12] Hiroyoshi Suzuki, Asako Kuwano, and Thant Htun. *Numerical Motion Analysis of ROV Applying ANCF to Tether Cable Considering Its Mechanical Property*. International Ocean and Polar Engineering Conference. ISOPE, June 2018.

[13] C.M. Ablow and S. Schechter. Numerical simulation of undersea cable dynamics. *Ocean Engineering*, 10(6):443–457, January 1983.

[14] Chenyu Zhao, Philipp Thies, and Lars Johanning. Offshore inspection mission modelling for an ASV/ROV system. *Ocean Engineering*, 259:111899, July 2022.

[15] Fan Xu, Hesheng Wang, Kwok Wai Samuel Au, Weidong Chen, and Yanzi Miao. Underwater Dynamic Modeling for a Cable-Driven Soft Robot Arm. *IEEE/ASME Transactions on Mechatronics*, 23(6):2726–2738, December 2018.

[16] Pedro Abreu, Hélio Morishita, António Pascoal, Jorge Ribeiro, and Henrique Silva. Marine Vehicles with Streamers for Geotechnical Surveys: Modeling, Positioning, and Control. *IFAC-PapersOnLine*, 49(23):458–464, 2016.

[17] Federico Renda, Michele Giorelli, Marcello Calisti, Matteo Cianchetti, and Cecilia Laschi. Dynamic Model of a Multibending Soft Robot Arm Driven by Cables. *IEEE Transactions on Robotics*, 30(5):1109–1122, October 2014.

[18] C. Viel. Self-Management of ROV Umbilical Using Sliding Buoys and Stop. *IEEE Robotics and Automation Letters*, 7(3):8061–8068, July 2022.

[19] Xiaohan Chen, Bing Liu, and Guigao Le. Numerical Simulation Research on the Anchor Last Deployment of Marine Submersible Buoy System Based on VOF Method. *Journal of Marine Science and Engineering*, 10(11):1681, November 2022.

[20] Shaowei Zhang, Chuan Tian, and Fenghua Zhou. Ocean observation system design of mooring buoy and benthic node with electro-optical-mechanical cable. *Frontiers in Marine Science*, 9:1018751, October 2022.

[21] J.L. Tang, G.X. Ren, W.D. Zhu, and H. Ren. Dynamics of variable-length tethers with application to tethered satellite deployment. *Communications in Nonlinear Science and Numerical Simulation*, 16(8):3411–3424, August 2011.